TECHNISCHE MECHANIK
European Journal of Engineering Mechanics
Diamond Open Access
journal homepage: www.ovgu.de/techmech

Tech. Mech., Vol. 46, Is. 1, (2026), 136–148
Received: 08.11.2025
Accepted: 09.02.2026
Available online: 16.02.2026

Design and Validation of a Pump Test Rig for Tribological and Thermal Analysis of Mechanical Seals Toward Condition Monitoring Development

David Heel[1]*, Peter Meusburger[1], Helmut Benigni[1], Johannes Bauer[2], Ferdinand Werdecker[2] and Maximilian Raith[2]

[1] Institute of Hydraulic Fluid Machinery, Graz University of Technology. Kopernikusgasse 24/4, A-8010 Graz
[2] EagleBurgmann Germany, Äußere Sauerlacher Str. 6-10 D-82515 Wolfratshausen

Abstract: This paper presents the design and implementation of an experimental pump test rig for investigating mechanical seals. The primary objective of the rig is to conduct long-term tests under varying operating parameters, providing a platform for developing condition monitoring systems for mechanical seals under realistic conditions. The adjustable parameters include pump speed, flow rate, system pressure, and water temperature at the pump inlet. Additionally, the design enables controlled air injection on the suction side, the simulation of dry-running of the seal, and the resulting thermal shocks during automatic refilling of the circuit, allowing replication of entire industrial processes. By incorporating vibrations, shocks, and other disturbances generated by the pump, the test rig provides a more comprehensive testing environment compared to conventional spindle-based rigs. It supports both automatic and semi-automatic operation modes, enabling comprehensive evaluation of condition monitoring systems and their practical applicability.

Initial measurement data demonstrate the correlation between pump-specific and seal-specific parameters. The measurements illustrate the operating range of the pump based on characteristic curves obtained at various rotational speeds. In addition, further measurements were conducted to investigate the influence of different operating conditions on the seal face temperature.

Keywords: Automatic operation, Condition monitoring, Long-term testing, Mechanical seals, Pump test rig

1 Introduction

Mechanical seals are high-precision sealing systems specifically developed for pressurized shaft passages. They are characterized by a very narrow sealing interface and low friction. Due to their low-maintenance design and long service life, they are widely used in pumps, compressors, propeller shafts, mixers, and filtration systems Schlegel (1984); Zhang et al. (2014). A study by the Fraunhofer Institute identified that the mechanical seal is one of the main reasons for the failure of pumps in industrial processes, followed by bearing and gap wear, as reported by Kohlmann and Schneider (2010).

Although mechanical seals are designed for long service lives, analysing premature failure or excessive wear remains a significant challenge. The unpredictability of such failures poses the risk of unplanned plant shutdowns, which can result in costs of several million euros per day, depending on the plant's size and production volume (SIEMENS AG, 2024). In many cases, repair and associated costs can surpass the initial cost of the seal by factors ranging from 100 to 1000 times (Riedl, 2017). Continuous condition monitoring is therefore a key research focus to detect wear and seal failure at an early stage, enabling planned maintenance and replacement cycles, and ensuring the operational reliability and cost-effectiveness of the entire system. Furthermore, API 682 (2014), which defines the requirements for shaft sealing systems in centrifugal and rotary pumps in the field of oil-, gas- and process engineering, mandates three years of uninterrupted operation while complying with environmental emission regulations. To meet these standard requirements, condition monitoring of the mechanical seal may be essential. The sealing interface of a mechanical seal is oriented normally to the shaft and is formed by two opposing faces. These surfaces are designed to allow a thin lubricating film to be established under specific operating conditions. The thickness of which significantly influences both leakage and frictional behaviour (Czichos and Habig, 2020). Leakage occurs radially through the sealing interface. To better understand the function of a mechanical seal, refer to Figure 1, which illustrates its schematic structure. The axially movable rotating seal face is pressed against a stationary seat by suspension element. This spring ensures automatic adjustment of the sealing interface, compensating for wear and thermal expansion, thereby maintaining continuous contact between the sealing face and the seat. Material pairings such as carbon graphite combined with metal or ceramic are often selected, while O-rings are employed as secondary sealing elements (Müller and Nau, 2024).

Previous efforts to develop condition monitoring systems have predominantly utilized spindle test rigs, where the seal is installed in a dedicated test setup and the shaft is driven externally. The test rig presented in this publication enables the development of condition monitoring systems directly within a pump. In addition to facilitating the design of new monitoring approaches, it also allows for the evaluation of existing condition monitoring systems. By precisely controlling the operating conditions, specific processes and events can be conducted in a reproducible manner.

* E-mail address: david.heel@tugraz.at
doi: 10.24352/UB.OVGU-2026-014

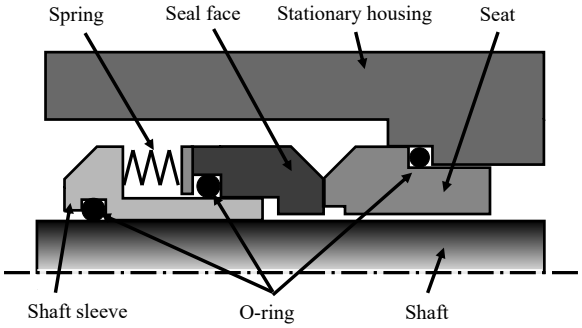

Fig. 1: Schematic design of a mechanical seal

2 Failure of Mechanical Seals

2.1 Theory of wear

When defining the tribological system of a mechanical seal based on DIN 50320 (1979), the stationary seat serves as the base body, while the rotating seal face acts as the counterbody, which is subjected to the applied load. Depending on the configuration of the seal, the barrier fluid or the ambient air acts as the environmental medium. In general, frictional states can be classified into solid-state friction, boundary friction, mixed friction, fluid friction, which includes hydrostatic, hydrodynamic, and elastohydrodynamic lubrication, as well as gas friction, which can occur under aerostatic or aerodynamic conditions. All of these frictional states can occur within a mechanical seal, leading to different wear mechanisms. The most common wear mechanisms include adhesion, abrasion, surface fatigue, and tribochemical reactions (Czichos and Habig, 2020).

According to Popov (2015), the dominant wear mechanism in sliding contacts is adhesive wear. Continuous stress on the sliding surfaces due to adhesive contact leads to crack formation at the surface unevenness. If adhesion forces become too high, particles or material grains may detach. These particles are further ground down within the sealing gap until they are flushed out, causing additional cracks and leading to material removal (Popov, 2015; Ni et al., 2023).

The wear volume V_{wear} can be determined using the Holm–Archard equation Archard (1953), which states that the worn volume is proportional to the normal force F_{N} and the sliding distance x, while being inversely proportional to the hardness σ_0 of the softer sliding partner. Manufacturers typically provide the dimensionless wear coefficient K_{wear} based on the material pairing:

$$V_{\text{wear}} = K_{\text{wear}} \frac{F_{\text{N}}\, x}{\sigma_0} \tag{1}$$

2.2 Premature failure

A mechanical seal is a wear component designed for a specific service life. The primary factor used to determine its lifespan is the adhesive wear of the sealing surfaces. However, a significant amount of mechanical seals does not reach their expected service life. In such cases, the term ”premature failure” is used (Fan, 2007). There are numerous reasons why a mechanical seal may fail before reaching its intended lifespan. Some of these factors occur even before the seal is put into operation, including design flaws, manufacturing defects, or installation errors. Regardless of these pre-operational issues, this discussion focuses on failure mechanisms that arise during operation. In many cases, premature failure is caused by a combination of multiple factors rather than a single issue (Plumridge and Page, 1992).

2.2.1 Mechanical overload

Even with proper design and installation, a mechanical seal may experience excessive mechanical stress. One of the primary causes is operational misuse of the equipment. Excessive pressure or sliding speeds can lead to grooving on the sealing surfaces (Riedl, 2017). Sudden pressure surges, often resulting from the rapid closing of a valve or shut-off device, can impose shock loads on the seal, potentially causing cracks or edge chipping. Additionally, mechanical overload can be induced by pump vibrations, whereas damaged bearings may cause these vibrations. Furthermore, improper flow conditions, such as blockages, deposits, or unfavourable operating points, can lead to increased radial forces acting on the seal, further accelerating wear and failure (Shiels, 2002a).

2.2.2 Thermal overload

One of the leading causes of thermal overload is dry-running of the seal, which can lead to fluid evaporation within the seal chamber (Fan, 2007). A sudden temperature change, such as flushing the system with a cold medium after a high-temperature process, can cause thermal shock. Similarly, irregular operating conditions, including frequent start-stop cycles or insufficient flushing, can result in excessive heat build-up (Shiels, 2002b). The consequences of thermal overload include crack formation, material embrittlement, and deformation of sealing components (Mayer, 1960). Moreover, excessively high temperatures can also cause degradation of secondary seals such as O-Rings, leading to leakage and failure of the entire sealing system.

2.2.3 Chemical degradation

Mechanical seals are also vulnerable to chemical attacks, particularly corrosion of metallic or ceramic components (Riedl, 2017). Additionally, carbonization or crystallization of process media can lead to increased leakage or even complete seal failure (Müller and Nau, 2024). Secondary seals, may also be compromised if the material compatibility with the process fluid is insufficient. Chemical degradation is particularly critical in aggressive operating environments where exposure to acids, solvents, or high-temperature fluids accelerates material deterioration.

3 Condition monitoring for mechanical seals

The condition monitoring of mechanical seals can take various forms and must be tailored to the specific application. As previously discussed, there are numerous causes of seal failure. The first step in developing an effective monitoring system is to determine which failure mechanisms should be observed. Furthermore, the focus during development should always be on application in real use cases. A basic method for assessing the condition of a mechanical seal is leakage detection. Additional measurable parameters that provide insights into the frictional state include temperature measurements at the seal face, seat, or within the sealing gap (Fan, 2007). In particular, during solid-state friction and boundary lubrication, wear is significantly increased due to the conversion of kinetic energy into heat at the tribological contact interface. As a result, the temperature of the entire tribosystem and especially the interfacial temperature rises (DIN 50320, 1979). To assess the stress conditions acting on the seal, comprising a combination of pressure and sliding velocity (pressure x velocity), it is necessary to measure the operating pressure and rotational speed of the system (Fan et al., 2008, 2013). Lambert (1998) already presented a system which monitors the condition of mechanical seals by measuring operating parameters in 1998. To improve reliability, the surface temperature was calculated using a finite element method.

Beyond these basic condition monitoring techniques, measuring the lubrication film thickness within the sealing gap provides valuable information on the friction state of the sliding surfaces. By defining a critical threshold for fluid film thickness, a distinction can be made between pure fluid lubrication and solid-state contact (Fan et al., 2013). Since the fluid film is only a few micrometers thick, the sensors used must have a very high resolution. However, measuring the lubrication film thickness is particularly challenging in transient operating conditions, where temperature variations further complicate the measurement task.

Several sensor-based measurement techniques have been investigated for determining the lubrication film thickness, for example by Zou and Green (1998) using an eddy current sensor. The eddy current proximity probes were attached to the end of the housing to measure the static and dynamic distance between the seat and the end face of the rotor.

Another possibility is to use the acoustic emission signal (AE), as this can contain a lot of information on the friction of the end surfaces. Based on the operating conditions, three main mechanisms can contribute to AE generation during sliding, namely viscous friction due to the shearing of lubricant layers, the interaction between surface irregularities and fluid flows, and direct contacts of the surface irregularities. In addition to understanding the formation mechanism of tribological AEs in mechanical seals, there is a difficulty in characterizing the AE signal (Towsyfyan et al., 2019; Fan et al., 2008). A further option is to impose active ultrasonic waves with a piezoelectric ultrasonic transducer and compare them with the signal reflected and received by the sliding surface (Fan et al., 2008). The theoretical principles governing the interaction of ultrasound with the interfaces and the fluid film are presented by Dwyer-Joyce (2005).

The above list provides a brief overview of the possibilities for condition monitoring. There are many other promising methods. For future research, there are improvements in sensor accuracy, the integration of real-time monitoring systems, and the optimization of data analysis techniques to implement.

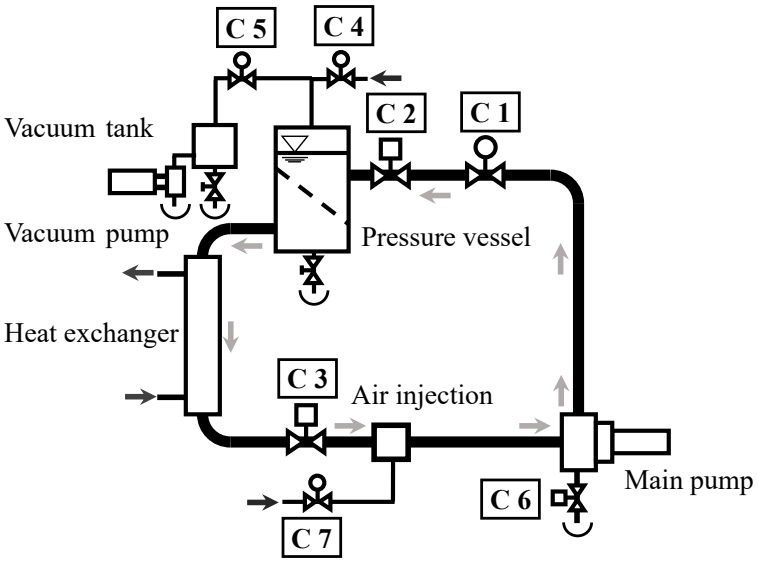

Description	ID
Flow control valve	C1
Butterfly valve pressure side	C2
Butterfly valve suction side	C3
Pressure boost valve	C4
Pressure relief valve	C5
Pump drain valve	C6
Air injection control valve	C7

Fig. 2: Schematic diagram of main test rig components

4 Test rig

The primary circuit, also referred to as the main circuit, is driven by the main pump and is shown schematically in Figure 2. The corresponding test rig is shown in Figure 3. The test mechanical seals ensure that the medium in the main circuit is sealed against the environment in particular the rotating shaft of the main pump against the housing.

Following the flow direction from the main pump, the medium passes through a flow control valve (C1), which regulates the volumetric flow rate, before entering the pressure vessel. The pressure vessel serves as a damping element, with an adjustable air cushion in the upper half that allows system pressure modulation. From there, the medium continues its way through a heat exchanger, which allows precise thermal conditioning, before flowing through a dedicated pipeline section designed for controlled air injection. Finally, the medium returns to the pump inlet, closing the loop. To simulate dry-running conditions, the pump's drainage valve (C6) can be opened, enabling controlled evacuation of the working fluid. Butterfly valves (C2) and (C3) are installed on the suction side and the pressure side of the main pump. When closed, they prevent complete drainage of the system, ensuring that only the section between the valves is emptied.

4.1 Control variables of the test rig

The test rig can operate fully automatic, with predefined process steps being executed sequentially. Alternatively, a semi-automatic mode allows for manual input of specific control variables. The following sections describe the individual control loops.

The drive motor of the main pump is controlled via a frequency converter, which regulates and monitors the motor operation. The actual speed is measured by a rotary encoder (M15) that records the rotational speed of the motor shaft. The flow rate in the primary circuit is regulated using a proportional valve (C1). By adjusting the valve position, the volume of liquid flowing through the main circuit can be continuously controlled. A magnetic inductive flow meter (M06) is used to measure the flow rate. To ensure the possibility of reducing the flow to zero discharge, a shut-off valve is installed in the primary circuit. The system pressure is regulated via an air cushion in the upper section of the pressure vessel. To increase pressure, compressed air from an external supply is introduced via the booster valve (C4), expanding the air cushion until the desired pressure is reached. Pressure reduction is achieved via the pressure relief valve (C5), which is connected to a vacuum tank. This allows air to be released from the pressure vessel into the vacuum tank, which is maintained at a reduced pressure by a vacuum pump. The actual system pressure is recorded by the piezoresistive pressure sensor (M03). The temperature in the primary circuit is regulated via a heat exchanger, which dissipates excess heat. The setpoint temperature is determined by sensor (M09), a PT100 resistance thermometer. The cooling source of the system is a chiller unit, while heat is introduced into the system through the operation of the main pump.

The test rig allows for controlled air injection into the main circuit on the suction side of the pump. This is achieved via a pipe section equipped with mixing nozzles. The pipeline assembly consists of an annular chamber with wall perforations, which is connected to a pressurized air line equipped with a check valve. The air flow rate is regulated using proportional valve (C7) and monitored via an ultrasonic flow meter (M08).

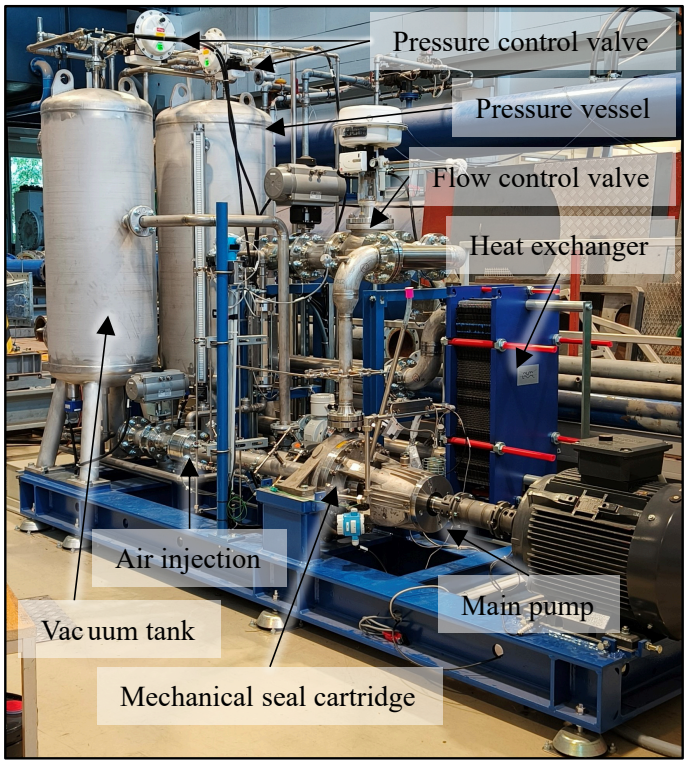

Fig. 3: Test rig overview

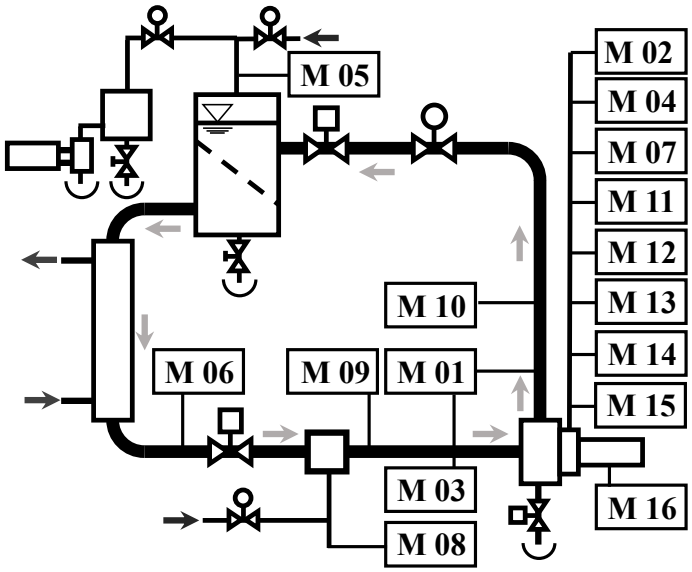

Pressure		
Differential pressure pump	$p_{\text{diff, Pump}}$	M01
Relative pressure at seal	$p_{\text{rel, Seal}}$	M02
Absolute pressure suction side	$p_{\text{abs, SS}}$	M03
Absolute pressure ambient	$p_{\text{abs, Amb}}$	M04
Relative pressure pressure vessel	$p_{\text{rel, PV}}$	M05
Flow rate		
Main circuit	Q	M06
Flush mechanical seal	Q_{Flush}	M07
Air injection	Q_{Air}	M08
Temperatures		
Suction side	T_{SS}	M09
Pressure side	T_{PS}	M10
Flush mechanical seal	T_{Flush}	M11
Seat product side	T_{SP1}	M12
Seat atmosphere side	T_{SA2}	M13
Barrier fluid	T_{BF}	M14
Rotational speed		
Main pump speed	n	M15
Electrical power		
Main pump power	P	M16

Fig. 4: Diagram of the instrumentation and corresponding measured variables at the test rig

4.2 Mechanical seal

The investigated component is a double mechanical seal arranged in a tandem configuration, designed and built as a cartridge unit, as illustrated in Figure 5. The seal faces are manufactured from carbon graphite, while the seat is built out of silicon carbide. The seal is supplied according to API 682 (2014) Plan 11, in which part of the product is diverted from the pressure side (PS) of the pump through a bypass line to the seal chamber. The flush flow through the seal is indicated by arrows in Figure 5. The purpose of this arrangement is to remove the frictional heat generated at the seal faces, flush out particles, and ensure adequate lubrication of the sliding surfaces. Between the two mechanical seals, a barrier fluid (BF) is provided and connected to a seal support system according to API 682 (2014) Plan 53A. This closed, pressurized barrier system with an external reservoir supplies the seal with a clean barrier medium. For the initial tests, the reservoir was operated at atmospheric pressure only. Since the test rig operates under positive pressure, any potential leakage would occur from the process side toward the barrier fluid. Circulation of the barrier fluid is achieved by a pumping ring integrated in the seal cartridge. No active cooling was installed for the first test series, meaning that the temperature in the reservoir was mainly influenced by the frictional heat at the seal faces and the temperature of the main process circuit. Deionized water is used in both the main circuit and the barrier fluid.

4.3 Condition monitoring of the mechanical seal

As shown in Figure 4, a set of measurement variables is extracted from the main pump, representing the condition monitoring system of the mechanical seal. The monitored parameters include the relative pressure at the seal (M02) and the ambient pressure (M04) as the key pressure indicators. The flow rate in the flushing line from the spiral casing to the seal is measured by an ultrasonic flow meter (M07). Additional monitored variables comprise the temperature in the flushing line (M11), the seat temperature on the product side (M12), the seat temperature on the atmosphere side (M13), and the temperature of the barrier fluid (M14). The rotational speed of the main pump (M15) is also recorded to complete the measurement set required for defining the load collective. Figure 5 provides an overview of the spatial arrangement of the individual measurement points. The selected monitoring parameters represent fundamental baseline values. However, the system allows for future expansion. Before extending the monitoring setup, it is essential to determine the specific tests to be conducted on the test rig. If necessary, additional parameters can be integrated into the condition monitoring system.

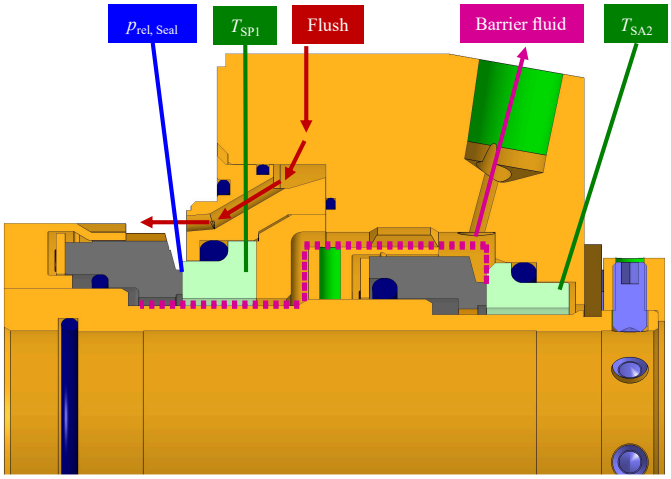

Fig. 5: Instrumentation of the mechanical seal

5 Initial measurement data

For this study, three measurement series were recorded, each representing a pump characteristic curve. The pump characteristics were determined at three constant rotational speeds: 1500 rpm, 2500 rpm, and 3500 rpm. In addition, for each measurement series the system pressure was maintained at 6 bar, and the temperature was kept constant at 20 °C on the suction side of the pump. Starting from zero discharge, the flow rate was incrementally increased in steps of 10 m^3/h until the pump's maximum achievable flow rate was reached. The pump delivery head is determined by the aforementioned parameters. The process sequence executed on the test rig ensures that the system is properly prepared before the actual measurement. Before recording a pump characteristic curve, the pipeline system is flushed, and the test rig is stabilized at a constant temperature of 20 °C. Therefore, the main pump speed is set to 2500 rpm, and a flow rate of 80 m^3/h is held constant for 200 s. Following this stabilization phase, an automated flushing of the pressure sensors is performed at reduced speed. After completing this step, the actual measurement process is initiated. In the final stage, the pump speed is brought to a full stop at 0 rpm. This standardized procedure ensures repeatable initial conditions for each test run, thereby improving the reliability and reproducibility of the measurements. Each measurement series was recorded continuously. The measuring software sampled data at 1000 Hz and stored averaged values every second.

Figure 6 (top) illustrates the complete process sequence for the measurement series at 2500 rpm. The graph (bottom) in Figure 6 shows the time interval of the initial section of the characteristic curve at a flow rate of 0 m^3/s. Each process step consists of a settling phase and a holding phase. This is indicated by three vertical lines: the first marks the start of the process step and the

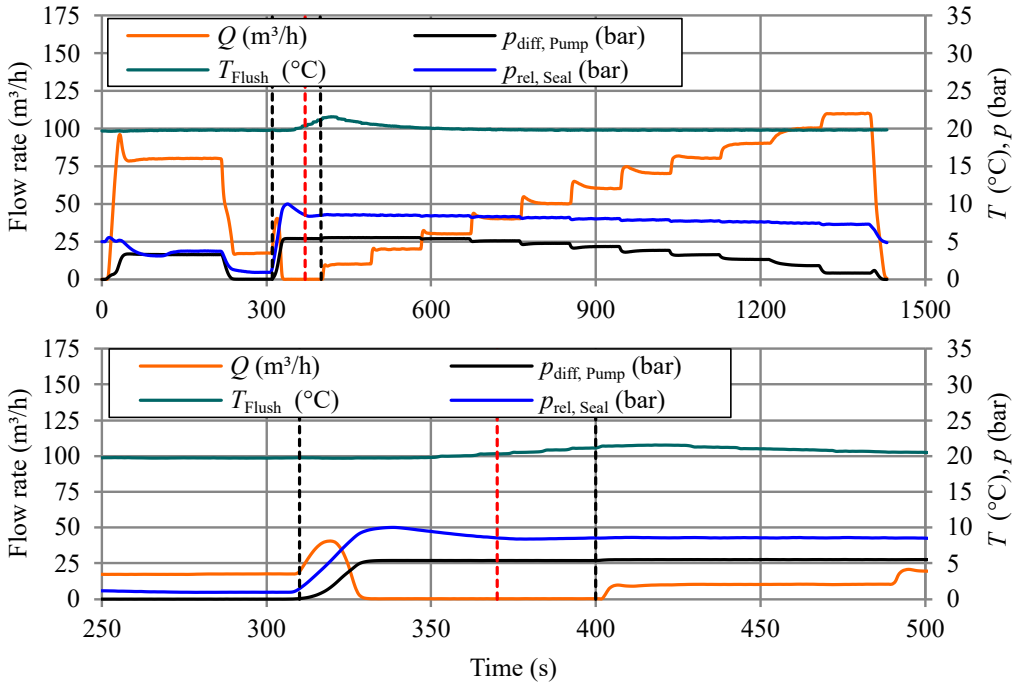

Fig. 6: Continuous recording at 2500 rpm, (top) full measurement log (bottom) first process step

beginning of the settling phase, the second marks the transition from the settling to the holding phase, and the third marks the end of the holding phase and the completion of the process step. During the settling phase, the control system adjusts the operating parameters until they stabilize. In the holding phase, the values reached at the end of the settling phase are maintained. If the target system pressure is 6 bar but only 4.5 bar is achieved within the predefined settling time, then 4.5 bar becomes the new target value for the holding phase. As a result, no significant changes occur during the holding phase, allowing for the calculation of an average value $\bar{x}$ that is representative of this operating state of the pump while minimizing variance. For the measurement series, the settling phase duration was set to 60 s, followed by a holding phase of 30 s.

In Figures 7 to 9, a mean value was calculated from the data recorded during the retention phase, representing a single measurement point. The authors consistently present the data as a set of two graphs. The left graph illustrates the pump characteristic curve at the respective rotational speed, along with the pump efficiency and the measured electrical power, compensated by the efficiency of the drive motor. By analysing the pump characteristic curve, its power and its efficiency, the operating point of the pump can be assessed. This evaluation also serves to associate the data related to the seal, which is depicted in the right graph. For the seal-related data, the selected parameters include the sealed pressure, as well as the flow rate and temperature of the flushing

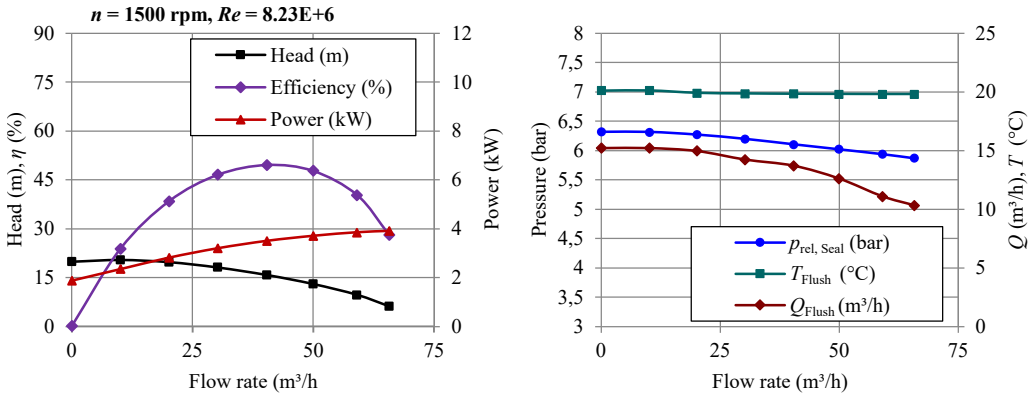

Fig. 7: (left) Pump characteristic 1500 rpm, (right) corresponding measured seal variables

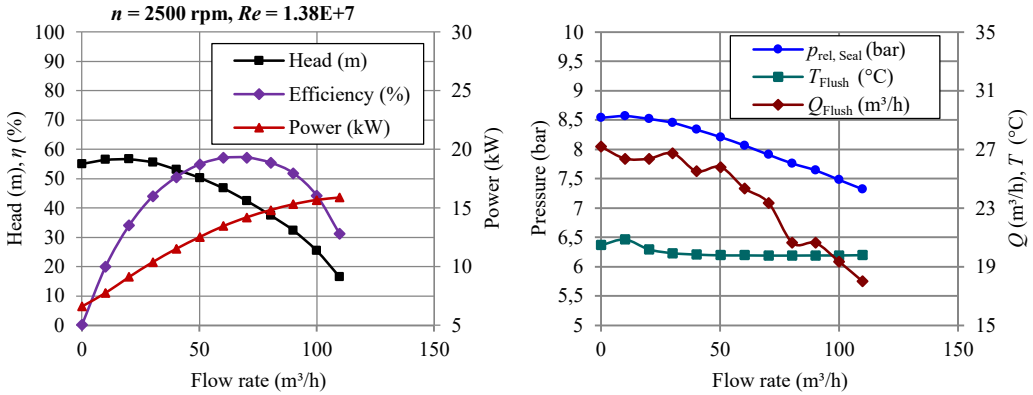

Fig. 8: (left) Pump characteristic 2500 rpm, (right) corresponding measured seal variables

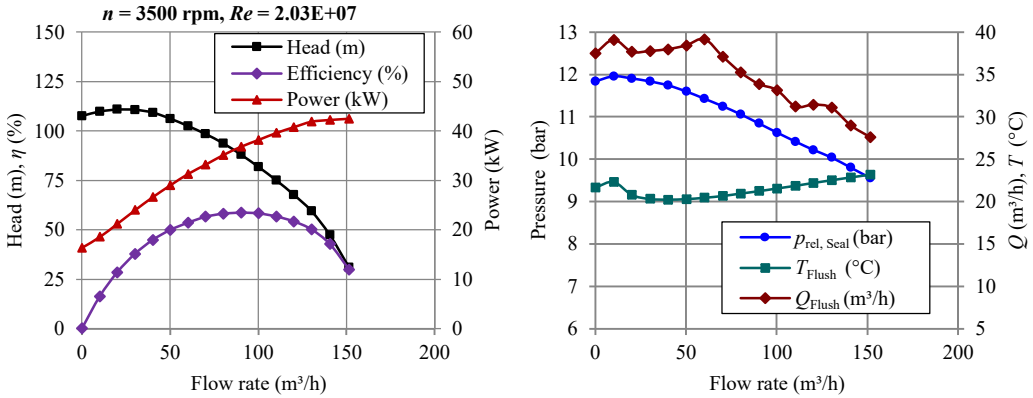

Fig. 9: (left) Pump characteristic 3500 rpm, (right) corresponding measured seal variables

medium. All data are plotted against the flow rate. Based on these representations, the following section analyses the trends observed in the measurement data, focusing on the interaction between pump and seal.

The results, as shown in Figure 7, illustrate the pump's performance at a rotational speed of 1500 rpm. At this speed, the pump reaches a maximum head of 20.4 m and a maximum flow rate of 65 m^3/h, with a peak efficiency of 49.6 %. Examining the head curve from the first measurement series reveals that the second measurement point is slightly above the first. Gülich (2020) describes characteristic curves where the gradient $\partial H/\partial Q > 0$ as "unstable." The drop in head at very low flow rates can be attributed to recirculation within the impeller, a typical behaviour for centrifugal pumps of this specific speed and design. The power and efficiency curves both follow the expected trends. The relative pressure at the seal decreases as the flow rate increases, which is expected since the pump head also decreases. Notably, the entire pressure generated by the pump does not appear at the seal. This drop in static pressure can be explained by the dynamic pressure component, which is influenced by the flushing flow. The dynamic pressure reduction occurs due to the flushing flow, which follows an inverse trend compared to the main pump flow. The flushing line functions as a bypass from the spiral casing to the seal, meaning that the higher the differential pressure generated by the pump, the higher the flushing flow rate. The temperature of the flushing flow remains constant at 20 °C, which is consistent with the suction-side temperature regulation of the pump.

Figure 8 presents the data from the measurement series at 2500 rpm. At this rotational speed, the pump achieves a maximum head of 56.6 m and a maximum flow rate of 109.7 m^3/h. By applying the similarity laws according to DIN EN ISO 9906 (2012) or IEC 60193 (2019), similar operating points can be converted. In this context, the flow rate scales linearly to the speed ratio, the head scales to the square of the speed ratio, and the power scales to the cube of the speed ratio. Applying these laws to the measurement data reveals a good correlation between the first and second measurement series. The pump reaches a peak efficiency of 57.2 %, which is significantly higher than the efficiency measured in the first series. According to IEC 60193 (2019), the frictional losses in the flow of hydraulic machinery are primarily dependent on the Reynolds number (Re). Since the Reynolds number increases by approximately 1.7 times due to the higher rotational speed, an increase in efficiency is also expected. It should be noted that the outlet diameter of the impeller was used as the characteristic length for calculating the Reynolds number shown in Figures 7 to 9. In Figure 8, the pump exhibits an unstable characteristic curve according to Gülich (2020) and the API 682 (2014). The relative pressure at the seal follows a trend similar to that observed in the first measurement series, and the unstable nature of the pump characteristic curve is also evident in the pressure profile. The temperature of the flush remains at approximately 20 °C, with a slight increase observed at very low flow rates. This temperature rise occurs because, at this operating point, thermal energy accumulates due to insufficient dissipation caused by the low flow rate. Examining the temporal progression in Figure 6 shows a continuous temperature increase once a flow rate of 0 m^3/h is reached. As previously discussed, the standardized startup process ensures that this temperature increase does not originate from prior process conditions.

The data from the latest measurement series at 3500 rpm are shown in Figure 9. At this rotational speed, the pump achieves a maximum head of 110.9 m, a maximum flow rate of 151.6 m^3/h, and a peak efficiency of 58.7 %. The correlation based on the similarity laws aligns very well with the other measurement series. The trend of the relative pressure at the seal and the flushing flow rate fits the overall pattern. The temperature profile of the discharge through the flushing line shows a slight increase at very low flow rates, subsequently drops back to 20 °C, and then rises steadily. A possible explanation for this behaviour could be the power increase, which scales with the cube of the rotational speed ratio. This causes the pump housing and the cartridge to heat up over time until a thermal equilibrium is reached.

To complement the presented measurement results, Table 1 provides quantified uncertainty values for the displayed parameters. The uncertainty analysis follows DIN EN ISO 9906 (2012), using representative values near the pump's best efficiency point. Measurement uncertainty may vary across the measurement range, particularly at its boundaries, where deviations tend to be more pronounced. The primary objective is to provide a quantitative estimate of the uncertainty associated with the reported values. The analysis accounts for the entire measurement chain, including the data acquisition system, galvanic isolation amplifiers, signal conditioners, and the respective sensors. The reported uncertainties represent expanded uncertainties with a confidence level of 95 %. The current setup meets the grade 1 acceptance criteria for pump measurements according to DIN EN ISO 9906 (2012).

6 Investigation of seat temperature at various operating conditions

The author presents two measurement series to investigate the relationship between the seal face temperature and the operating conditions. The instrumentation of the mechanical seal has been shown in Figure 5, and the overall measurement setup is illustrated in Figure 4. The temperature is measured at the seat of the sealing on the product side as well as at the seat on the atmosphere side. The uncertainty of the measured parameter was evaluated based on manufacturer specifications. It includes contributions from the sensors, signal conditioning, and data acquisition chain. Table 1 summarizes the relevant measurement uncertainties associated with the recorded parameters. In the first series of the measurements, the rotational speed is varied. Since the delivery head of the pump depends on the rotational speed, the system pressure must be counterbalanced to ensure that only the influence of speed is examined. In the second series, the relative pressure at the seal is varied by changing the system pressure operated at constant speed and therefore at constant head.

The thermal power generated at the seal faces can be determined using the friction torque T_r and the rotational speed n according to the following Equation 2, which can be found in the API 682 (2014).

$$P_R = T_r \cdot \frac{2\pi}{60} \cdot n \tag{2}$$

The friction torque of a mechanical seal can be determined according to API 682 (2014) using the following relationship (see Equation. 3), where p_{tot} is the total pressure acting on the seal faces, A is the effective sealing face area, f is the dynamic friction coefficient, and D_m is the mean seal face diameter. The total face pressure p_{tot} represents the sum of the hydraulic and mechanical loading acting on the seal faces. It is calculated from the relative pressure of the seal $p_{\text{rel, seal}}$, the balance ratio B, the pressure gradient factor $K_{\Delta\text{p}}$, and the specific spring pressure p_{sp}. The term $p_{\text{rel, Seal}} \cdot (B - K_{\Delta\text{p}})$ in Equation 4 describes the portion of the relative pressure at seal pressure transmitted to the seal faces, while p_{sp} accounts for the additional mechanical load applied by the springs.

$$T_r = p_{\text{tot}} \cdot A \cdot f \cdot \frac{D_m}{2} \tag{3}$$

$$p_{\text{tot}} = p_{\text{rel, Seal}} \cdot (B - K_{\Delta\text{p}}) + p_{\text{sp}} \tag{4}$$

Equations 2, 3 and 4 show that the dominant operating variables influencing the generated heat are the relative pressure at seal $p_{\text{rel, Seal}}$, the rotational speed n, and the dynamic friction coefficient f. The pressure drop coefficient $K_{\Delta\text{p}}$ is influenced by pressure, temperature, and the hydrodynamic conditions (rotational speed), but is assumed to be constant in this study. All other parameters are determined by the specific seal geometry and construction of the mechanical seal. According to the standard API 682 (2014), the dynamic friction coefficient f of a mechanical seal is typically discussed in the range of 0.01 to 0.18 under normal operating conditions. A more detailed analysis of the frictional state within the sealing interface could be performed by calculating the Gümbel number G, a dimensionless hydrodynamic parameter according to Waidner (2019). However, this aspect is not further considered here. The API 682 (2014) specifies a standard dynamic friction coefficient of $f = 0.07$, which is also assumed in this study. Based on this assumption, the parameters that influence the seal face temperature can be limited to the relative pressure at the seal and the rotational speed.

Tab. 1: Measurement uncertainty

Description	**Abbr.**	**Uncertainty [%]**
Head	H	0.71
Flow rate	Q	0.87
Efficiency	η	1.73
Power	P	1.32
Relative pressure at seal	$p_{\text{rel, seal}}$	0.80
Temperature (PT100)	$T_{\text{flush}}, T_{\text{SS}}$	0.82
Temperature (thermocouples)	$T_{\text{SP1}}, T_{\text{SA2}}, T_{\text{BF}}$	1.5715
Rotational speed	n	0.79
Flow rate (flush)	Q_{flush}	1.57

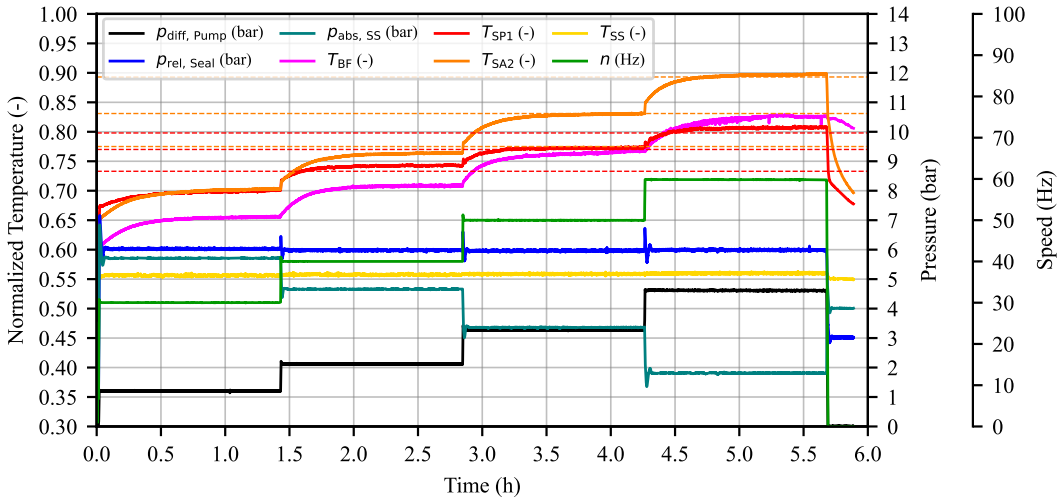

Fig. 10: Measurement series 1: variation of rotational speed n = 1800, 2400, 3000, 3600 rpm (30, 40, 50, 60 Hz) at constant relative seal pressure $p_{\text{rel, Seal}}$ = 6 bar.

A base operating point was defined for the pump at a rotational speed of 3600 rpm (60 Hz). The flow control valve opening was set to 60 % resulting in a pump flow rate of approximately 134 m^3/h and a differential pressure of 4.6 bar. Under these conditions, the discharge through the flush line was 3.2 m^3/h. The suction-side pressure was adjusted to 1.8 bar, yielding a relative pressure at the seal of 6 bar. The temperatures presented in this chapter are shown in a normalized form with reference to the maximum temperature observed in the measurement series. The temperature on the suction side is kept at a constant temperature for both measurement series. For this series of tests, the supply system is only pressurized to ambient pressure and the temperature of the barrier fluid is not actively controlled.

The first measurement series is shown in Figure 10. For this series, the rotational speed was increased from 1800 rpm (30 Hz) to 2400 rpm (40 Hz), 3000 rpm (50 Hz) and finally to the nominal operating point of 3600 rpm (60 Hz). Throughout this sequence, the system pressure was regulated so that the seal experienced a constant relative pressure of 6 bar at the product side. The pressure signal shows a distinct overshoot and undershoot at each transition, caused by the rapid change in speed. However, the control system quickly compensates for these deviations, and the pressure stabilizes again at 6 bar.
The switching points of the speed increments are also reflected in the seal temperature signals T_{SP1} and T_{SA2}, where a noticeable change in the slope of the curves can be observed until a new thermal plateau is established. It is further observed that the temperature of the barrier fluid T_{BF} follows the temperature trend of the seal seat at the atmospheric side T_{SA2}. This behavior is expected, as the barrier system is not actively temperature-controlled. In contrast, the temperature at the suction side of the pump T_{SS} remains constant throughout the entire measurement series. As discussed previously, the temperature behavior indicates a linear relationship between frictional power and rotational speed. Based on this approach, the temperature level for each speed step was estimated using the measurement data recorded immediately prior to the speed change. It is assumed that the overall temperature level of the seal is determined by both the operating conditions and the surrounding thermal environment. For this purpose, a reference temperature was defined for each seal by averaging the surrounding temperatures at the seal. On the product side, the reference temperature was calculated from the product temperature T_{SS} and the barrier fluid temperature T_{BF}, while on the atmospheric side it was obtained from T_{BF} and the ambient temperature T_{Amb}.
Using these reference temperatures, a temperature difference ΔT between the reference temperature and the measured seat temperature immediately prior to the speed change was determined. This temperature difference characterizes the increase in seal temperature and was subsequently scaled using the speed ratio. The predicted overall temperature level after the speed change was then obtained by adding the scaled temperature difference to the reference temperature.
As a representative example, the speed step from 1800 rpm to 2400 rpm is considered. On the product side, the reference temperature calculated from $T_{SS} = 0.559$ and $T_{BF} = 0.653$ yields $T_{ref,SP1} = 0.606$. The resulting temperature difference relative to the measured seat temperature $T_{SP1} = 0.701$ is $\Delta T = 0.095$, which leads to a predicted temperature of 0.733 after scaling with the speed ratio. This value is slightly below the measured temperature of $T_{SP1} = 0.743$. Applying the same procedure to the atmospheric side results in a reference temperature of $T_{ref,SA2} = 0.466$ and a predicted temperature of 0.779. The corresponding measured temperature is slightly lower, at $T_{SA2} = 0.764$.
The same procedure was applied to the following speed step to 3000 rpm. In this case, an almost perfect agreement between the predicted and measured temperatures was obtained on both the product side and the atmospheric side. For the final step from 3000 rpm to 3600 rpm, the predicted temperature matches the measured temperature very well on the atmospheric side, while the predicted temperature on the product side is slightly lower than the measured value, but still in an acceptable range.

In the second measurement series (Figure 11), the rotational speed was kept constant at 3600 rpm, while the relative seal pressure was varied by adjusting the system pressure. The pressure was increased from the defined reference value of $p_{rel,\,seal} = 6$ bar to 8 bar, 10 bar, and finally 11 bar. The sealing rings on the atmospheric side are subjected to the same mechanical load throughout

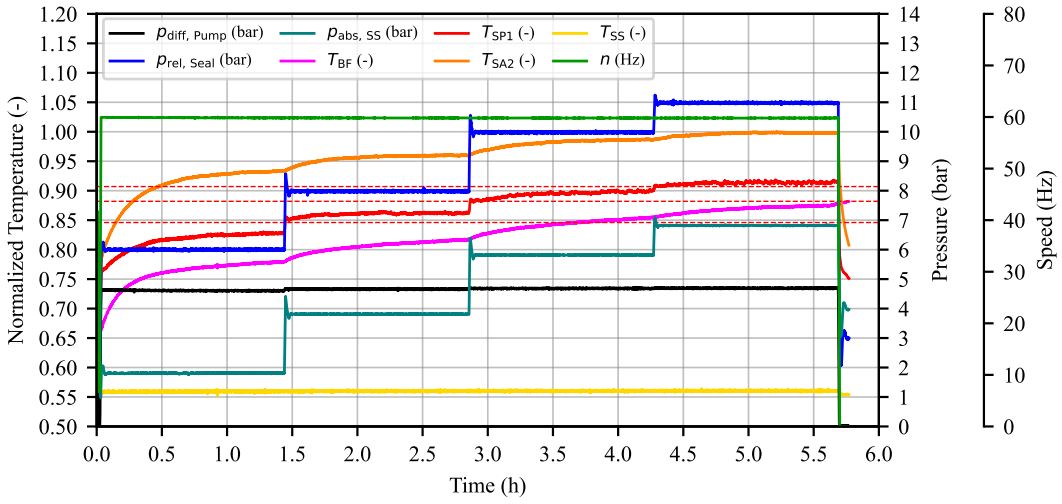

Fig. 11: Measurement series 2: variation of seal pressure $p_{rel,\,Seal} = 6, 8, 10, 11$ bar at constant rotational speed $n = 3600$ rpm (60 Hz).

the entire measurement series, as pressure control is applied exclusively on the product side of the seal within the main pump circuit. The observed temperature increase on the atmospheric side is therefore solely attributable to heat transfer from the product-side seal through the barrier fluid. Similar to the first measurement series, a slight overshoot in the pressure signal is observed in the measuremenat data during each transition. It is observed that the temperature level at the reference operating point in the first and in the second measurement series exhibits only limited repeatability. This applies to both the seat temperature on the product side and the seat temperature on the atmospheric side. The results show that in order to reliably predict the sliding temperature, the data measured immediately before a change in operating conditions must be used. One possible explanation is the temperature-related distortion of the seal face and seat during operation, as described by Waidner (2019). This leads to cyclic fluctuations in the friction torque and sliding temperature, as the effective pressure term $K_{\Delta p}$ changes slightly.

Similar to the previous series of measurements, the switching points can be clearly identified in the temperature profile, as the slope changes significantly. After each step, a settling phase is established until the steady-state temperature corresponding to the respective operating condition is reached. Again, a temperature difference ΔT was determined based on the reference temperature, and a prediction of the seal face temperatures was made. For this calculation, a $(B - K_{\Delta p})$ ratio of 0.22 and a representative spring pressure of $p_{sp} = 2.3\,\text{bar}$ were assumed. From these values, the total face pressure p_{tot} was determined as follows: for a relative seal pressure of $p_{rel,\,seal} = 6\,\text{bar}$, the total face pressure is $p_{tot} = 3.62\,\text{bar}$, for 8 bar it is $p_{tot} = 4.06\,\text{bar}$, for 10 bar it is $p_{tot} = 4.50\,\text{bar}$ and for 11 bar the corresponding value is $p_{tot} = 4.72\,\text{bar}$.

As a representative example, the pressure step from 6 bar to 8 bar is considered. The reference temperature calculated from $T_{SS} = 0.559$ and $T_{BF} = 0.778$ yields $T_{ref,SP1} = 0.668$. The resulting temperature difference relative to the measured seat temperature $T_{SP1} = 0.827$ is $\Delta T = 0.158$, which leads to a predicted temperature of 0.846 (first red dott line) after scaling with the speed ratio. This value is slightly below the measured temperature of $T_{SP1} = 0.863$. For all subsequent pressure steps, the predicted temperatures are consistently just beneath the measured values. This deviation can be attributed to gentle deformation of the sliding parts, which affects the pressure loss coefficient $K_{\Delta p}$, or to load-dependent fluctuations in the coefficient of friction f. Both effects would influence the frictional power and, consequently, the resulting sliding temperature.

In summary, a correlation between the seal face temperature and the operating point of the pump or seal has been demonstrated. The results show that changes in the temperature difference ΔT can be used to draw conclusions about the frictional state of the seal. Further measurements are required to determine whether this relationship also applies across the entire operating range of the seal and whether the temperature difference ΔT remains valid after prolonged operation.

7 Summary

Monitoring the condition of mechanical seals is essential for detecting wear and failures, ensuring operational reliability, and enabling early intervention. To develop and validate existing condition monitoring approaches for mechanical seals, a dedicated test rig was designed and constructed. The test rig allows precise control over key operating parameters, including pump speed, flow rate, system pressure, and water temperature at the pump inlet. Additionally, its design enables controlled air injection on the suction side, the simulation of seal dry-running conditions, and the resulting thermal shocks upon automatic refilling of the circuit. These features allow the replication of entire industrial processes under controlled conditions.

Initial measurements were recorded and analyzed using the pump performance curve as a reference. Further experiments investigated the relationship between the pump's operating point, the resulting operating point of the seal, and the seal face temperature. Strong correlations were observed, demonstrating that the operating behavior of the mechanical seal is closely linked to that of the pump and clearly illustrating the seal as an integral part of the overall system.

The presented test rig provides a solid foundation for further investigations, particularly long-term tests. Moreover, it can be employed to diagnose application-specific issues by replicating real-world processes in a controlled laboratory environment and applying appropriate measurement techniques to identify the root cause. The setup also facilitates the validation of existing condition monitoring systems, making it a versatile tool for research and practical applications. Future work will focus on optimizing the measurement techniques and further expanding the range of monitored parameters to further enhance the reliability of mechanical seal condition monitoring.

Acknowledgement

This research was conducted in cooperation between EagleBurgmann Germany GmbH & Co. KG and Technical University Graz. The authors gratefully acknowledge the financial support and technical collaboration provided by EagleBurgmann Germany GmbH & Co. KG throughout the project.

Authors' Contribution

All authors were involved in the conception and design of this study. D. Heel was responsible for material preparation, data collection, and analysis. D. Heel wrote the first draft of the manuscript, and all other authors provided feedback on previous versions. All authors read and approved the final manuscript.

Nomenclature

Symbol	Unit	Description	Symbol	Unit	Description
A	m^2	effective sealing face area	n	rpm	rotational speed
B	[-]	balance ratio	p_{abs}	Pa	absolute pressure
D_m	m	mean seal face diameter	$p_{abs,\,Amb}$	Pa	absolute ambient pressure
f	[-]	dynamic friction coefficient	$p_{abs,\,SS}$	Pa	absolute pressure at suction side
F_N	N	normal force	p_{diff}	Pa	differential pressure
G	[-]	Gümbel number	$p_{diff,\,Pump}$	Pa	differential pressure of the pump
H	m	pump head	p_{rel}	Pa	relative pressure
K_{wear}	[-]	wear coefficient	$p_{rel,\,PV}$	Pa	relative pressure at pressure vessel
$K_{\Delta p}$	[-]	pressure gradient factor	$p_{rel,\,Seal}$	Pa	relative pressure at seal
P	W	electrical power	p_{sp}	Pa	specific spring pressure
P_R	W	frictional power at seal faces	p_{tot}	Pa	total pressure acting on seal faces
Q	m^3/h	volumetric flow rate	Re	[-]	Reynolds number
Q_{Air}	m^3/h	air injection flow rate	T	°C	temperature
Q_{Flush}	m^3/h	flushing flow rate	T_{Amb}	°C	ambient air temperature
T_{Flush}	°C	flushing fluid temperature	T_{BF}	°C	barrier fluid temperature
T_{PS}	°C	temperature at pressure side	T_{SA2}	°C	seat temperature, atmosphere side
T_{SP1}	°C	seat temperature, product side	T_{SS}	°C	temperature at suction side
T_r	Nm	friction torque	V_{wear}	m^3	wear volume
x	m	sliding distance	η	%	efficiency
σ_0	N/m^2	hardness			

References

API 682. Pumps—shaft sealing systems for centrifugal and rotary pumps, 2014.

J. F. Archard. Contact and rubbing of flat surfaces. *Journal of Applied Physics*, 24(8):981–988, 1953. ISSN 0021-8979. doi: 10.1063/1.1721448.

H. Czichos and K.-H. Habig. *Tribologie-Handbuch*. Springer Fachmedien Wiesbaden, Wiesbaden, 2020. ISBN 978-3-658-29483-0. doi: 10.1007/978-3-658-29484-7.

DIN 50320. Verschleiß; Begriffe, Systemanalyse von Verschleißvorgängen, Gliederung des Verschleißgebietes, 1979.

DIN EN ISO 9906. Kreiselpumpen- Hydraulische Abnahmeprüfungen- Klassen 1, 2 und 3 (ISO 9906:2012); Deutsche Fassung EN ISO 9906:2012, 2012.

R. S. Dwyer-Joyce. The Application of Ultrasonic NDT Techniques in Tribology. *Proceedings of the Institution of Mechanical Engineers, Part J: Journal of Engineering Tribology*, 219(5):347–366, 2005. ISSN 1350-6501. doi: 10.1243/135065005X9763.

Y. E. Fan. *The condition monitoring of mechanical seals using acoustic emissions*. 2007. URL https://search.proquest.com/openview/d45754edc60d59500064fad3bd6a413f/1?pq-origsite=gscholar&cbl=2026366&diss=y&casa_token=jpfyyjkk-t8aaaaa:jsrdqm-l4spbcho3vd_s58nzg_mxbum4jg2nuhaeusgzrnhh9yunfquog9ihwv9k_ga30xlzbjy.

Y. E. Fan, F. Gu, and A. Ball. A review of the condition monitoring of mechanical seals. *ASME 7th Biennial Conference on Engineering Systems Design and Analysis*, pages 179–184, 2008. doi: 10.1115/ESDA2004-58229.

Y. E. Fan, F. Gu, and A. Ball. *A review of mechanical seal tribology and condition monitoring*. Proceedings of Computing and Engineering Annual Researchers' Conference 2013 : CEARC'13. University of Huddersfield, Huddersfield, 2013. ISBN 9781862181212. URL https://eprints.hud.ac.uk/id/eprint/19391/.

J. F. Gülich. *Centrifugal Pumps*. Springer International Publishing, Cham, 2020. ISBN 978-3-030-14787-7. doi: 10.1007/978-3-030-14788-4.

IEC 60193. Hydraulic turbines, storage pumps and pump-turbines – model acceptance tests, 2019.

B. Kohlmann and S. Schneider. Zuverlässigkeitsprognose von mechatronischen Systemen zur Ableitung restnutzungsdauerbezogener Betriebs- und Instandhaltungsstrategien. Final report, Fraunhofer-Institut für Materialfluss und Logistik IML, Dortmund, 2010. URL https://www.iml.fraunhofer.de/content/dam/iml/de/documents/OE%20240/10-12-20_ReMain_Abschlussbericht_final.pdf.

P. Lambert. A condition-based monitoring system for mechanical seals. *Sealing Technology*, 1998(57):7–9, 1998. ISSN 13504789. doi: 10.1016/S1350-4789(98)80013-5.

E. Mayer. Doppeltwirkende axiale Gleitringdichtungen in der chemischen Industrie. *Chemie Ingenieur Technik*, 32(4):285–288, 1960. ISSN 0009-286X. doi: 10.1002/cite.330320407.

H. Müller and B. Nau. Gleitringdichtungen: Grundlagen, 2024. URL www.fachwissen-dichtungstechnik.de.

X. Ni, J. Sun, C. Ma, and Y. Zhang. Wear model of a mechanical seal based on piecewise fractal theory. *Fractal and Fractional*, 7 (3):251, 2023. ISSN 2504-3110. doi: 10.3390/fractalfract7030251. URL https://www.mdpi.com/2504-3110/7/3/251.

J. M. Plumridge and R. L. Page. The development of more tolerant mechanical seals. In *Shaft Sealing in Centrifugal Pumps: Papers Presented at a Seminar Organized by the Fluid Machinery Committee of the Power Industries Division of the Institution of Mechanical Engineers, and Held at the Institution of Mechanical Engineers on 12 February 1992*, pages 9–22. Mechanical Engineering Publications for the Institution of Mechanical Engineers, London, 1992. ISBN 0-85298-811-7.

V. L. Popov. *Kontaktmechanik und Reibung*. Springer Berlin Heidelberg, Berlin, Heidelberg, 2015. ISBN 978-3-662-45974-4. doi: 10.1007/978-3-662-45975-1.

A. Riedl, editor. *Handbuch Dichtungspraxis*. Vulkan Verlag, Essen, 4. auflage edition, 2017. ISBN 3802722140.

R. Schlegel. Gleitringdichtungen für Pumpen in der chemischen Industrie. *Chemie Ingenieur Technik*, 56(5):397–399, 1984. ISSN 0009-286X. doi: 10.1002/cite.330560515.

S. Shiels. Failure of mechanical seals in centrifugal pumps — part two. *World Pumps*, 2002(432):34–37, 2002a. ISSN 02621762. doi: 10.1016/S0262-1762(02)80235-8.

S. Shiels. Failure of mechanical seals in centrifugal pumps. *World Pumps*, 2002(429):20–22, 2002b. ISSN 02621762. doi: 10.1016/S0262-1762(02)80169-9.

SIEMENS AG. The true cost of downtime 2024, 2024. URL https://assets.new.siemens.com/siemens/assets/api/uuid:1b43afb5-2d07-47f7-9eb7-893fe7d0bc59/TCOD-2024_original.pdf.

H. Towsyfyan, F. Gu, A. D. Ball, and B. Liang. Tribological behaviour diagnostic and fault detection of mechanical seals based on acoustic emission measurements. *Friction*, 7(6):572–586, 2019. ISSN 2223-7704. doi: 10.1007/s40544-018-0244-4. URL https://link.springer.com/article/10.1007/s40544-018-0244-4.

P. Waidner. *Gleitringdichtungen: Grundlagen und ihre Anwendung – der Versuch einer einfachen Erklärung*. buch.one Verlag Offsetdruckerei Grammlich, 2019. ISBN 9783947198115.

Z. Zhang, K. Chen, E. Q. Zhang, and P. Fu. Mechanical seal condition monitoring technology research. *Applied Mechanics and Materials*, 529:344–348, 2014. ISSN 1662-7482. doi: 10.4028/www.scientific.net/AMM.529.344. URL https://www.scientific.net/amm.529.344.

M. Zou and I. Green. Real-time condition monitoring of mechanical face seal. In D. Dowson, editor, *Tribology for energy conservation*, volume 34 of *Tribology Series*, pages 423–430. Elsevier for the Institute of Tribology University of Leeds and Institut National des Sciences Appliquées de Lyon, Amsterdam and New York, 1998. ISBN 9780444500335. doi: 10.1016/S0167-8922(98)80098-9.